Nonlinear seepage–erosion coupled water inrush model for completely weathered granite

Jinquan Liu, Weizhong Chen, Diansen Yang, Jingqiang Yuan, Xiaofei Li & Qingyan Zhang

Published online: 11 Oct 2017.

Submit your article to this journal ↗

View related articles ↗

View Crossmark data ↗

Taylor & Francis
Taylor & Francis Group

Check for updates

Nonlinear seepage–erosion coupled water inrush model for completely weathered granite

Jinquan Liu[a,b,c] (iD), Weizhong Chen[b,d], Diansen Yang[b], Jingqiang Yuan[b], Xiaofei Li[b,c], and Qingyan Zhang[b,c]

[a]Department of Geotechnical Engineering, School of Civil Engineering and Architecture, East China Jiaotong University, Nanchang, Jixangxi, China; [b]State Key Laboratory of Geomechanics and Geotechnical Engineering, Institute of Rock and Soil Mechanics, Chinese Academy of Sciences, Wuhan, Hubei, China; [c]University of Chinese Academy of Sciences, Beijing, China; [d]Geotechnical and Structural Engineering Research Center, Shandong University, Jinan, Shandong, China

ABSTRACT

Water inrush from completely weathered granite has presented a significant challenge for tunnel construction, suggesting the urgency and importance of revealing the water inrush mechanism. In this paper, a seepage erosion model is proposed to describe the water inrush. Assuming that completely weathered granite consists of solid grain phase, fluid phase, and fluidized grain phase, the three-phase interaction was constrained by mass balance equations, and the erosion of fluidized grains was described by a modified porosity evolution equation. The fluid flow is governed by a coupled Darcy–Brinkman/Navier–Stokes equation, which responds to the variation of the flow pattern in the evolution process. Then, the validity of the model has been proved, and the superiority has been studied by comparing with the previous models. The comparison results showed that the flow pattern has a significant impact on pore pressure, water velocity, and mutation time, and the proposed model can more accurately predict the development of velocity. Furthermore, this model was used to simulate the development of water inrush and achieved good results in predicting the direction, channel size, and whole evolution process of water inrush. The research findings from the paper can benefit tunnel engineering in the case of water inrush disasters.

Introduction

With the rapid development of transportation infrastructure, more and more tunnels are to be constructed in China. Unfavorable geology such as water-rich completely weathered granite, which is easy to induce water inrush disaster, is often encountered during the construction of subsea tunnels in southern China (Shin et al. 2011; Zhao, Li, and Tian 2013). Human casualties and property loss caused by water inrush are very serious at present. Tunneling in such conditions will be particularly difficult because of the potential for encountering mixed-face conditions, collapse, and erosion (Zhao, Gong, and Eisensten 2007; Zhang, Fang, and Lou 2014a; Shirlaw 2016). Over the last 40 years, much research has been devoted to studying the description, classification, weathering process, and engineering behavior of weathered rocks. Anon (1977) and Arıkan, Ulusay, and Aydın (2007) have developed a systematical description and classification of weathered rocks. Irfan (1997) studied the mineralogical characterization and classification of weathered granite. Six grades from fresh rock (Grade I) to residual soil (Grade VI) were adopted to classify weathered granites. The main minerals of fresh rock include quartz, feldspar, biotite, and hornblende. Weathering results in a loss of feldspar, leaving a material predominantly consisting of quartz particles and clay minerals such as kaolinite and montmorillonite as the weathering grade increases to completely weathered granite (Grade V). This material erodes rapidly and becomes weak and soil-like. Shirlaw, Hencher, and Zhao (2000) also claimed that the completely weathered rocks were prone to erosion when exposed because of little cementation. Under certain conditions, the quartz particles and clay minerals may be gradually eroded by groundwater flow, leading to the rapid increase in ground permeability and the formation of water channels, and ultimately the water inrush disaster. Undoubtedly, water inrush disasters have become a serious threat to the tunnel construction in completely weathered granite due to its special engineering behavior. So predicting the evolution of water inrush for an advance warning is very meaningful and urgent, but improvements in this area are seriously hindered due to the complexity of water inrush mechanisms.

Most previous studies related to the mechanism of water inrush were mainly in coal floors, fractured rock masses, and karst regions. For instance, to assess the risk of water inrush, many scholars have attempted to establish a correlation between the lithology, fractures, aquifuge thickness, and water inrush (Zhang and Shen 2004; Meng, Li, and Xie 2012; Li et al. 2013). In the 1960s, Chinese scholars proposed an empirical formula for the water inrush coefficient by selecting the aquifuge thickness and water pressure as two main factors

affecting water inrush. In practical application, this method oversimplifies the geological conditions and cannot accurately predict the probability of water inrush. In recent years, the underlying belt theory, plate model, and some other theories have been developed for water inrush assessment (Yang and Huang 2007; Wei et al. 2010; Tang et al. 2011). These methods have played a certain role in the risk assessment of water inrush, but they cannot reflect the formation mechanism of water inrush. The water inrush mechanisms for fractured rock masses and karst involve the initiation, extension, and perforation of cracks under different geological and hydrogeological conditions. Considering the rock damage properties, Valko and Economides (1994) studied the rock fracture process under the action of hydraulic fracturing. Wang and Park (2003) proposed a flow-stress coupling water inrush model based on an elastoplastic theory, in which the water inrush channel was determined only by the permeability evolution caused by rock deformation. Yang et al. (2007) developed a numerical model that involved the coupled effects of flow, stress, and damage. However, these are not appropriate for the weathered rock, especially for the completely weathered rock and residual soil due to the soil-like behavior. Completely weathered granite has a large amount of fine particles but little cementation, which makes them prone to disintegration and water erosion. Therefore, it is essential to reconstruct a suitable model for completely weathered granite considering the erosion behavior.

In this paper, a new coupled seepage erosion model was proposed based on theories of solute transport and fluid dynamics in porous media, which consists of mass balance equations, seepage equation, and porosity evolution law. The main processes of the new model are as follows: (a) suppose that completely weathered granite consists of the solid grain phase, fluid phase, and fluidized grain phase; the fluidized grain phase is considered to be a special solute that moves with the fluid. (b) The three-phase interaction is considered by combining their mass balance equations and a porosity evolution equation describing the erosion of fluidized particles, and the influence of eroded particles on the porosity and pore pressure is considered in the evolution of water inrush. (c) The non-linear water inrush mechanism was analyzed, and changes in the flow pattern in the evolution process were considered, including the Darcy flow in the initial flow stage, Brinkman flow in the rapid flow stage, and Navier–Stokes pipe flow in the final flow stage. The new model can predict the development of water inrush under complex boundary and flow conditions and reflects the dynamic evolution of particle loss, porosity, permeability, pore pressure, and water inflow induced by the erosion and migration of particles.

Seepage erosion coupled water inrush model for completely weathered granite

Basic assumptions and definitions

Basic assumptions: (1) completely weathered granite is considered as a three-phase system consisting of solid grains (sg), fluid (f), and fluidized solids (fs). The fluidized grains are considered to be a special solute that moves with the fluid.
(2) The pore spaces are completely filled with fluid and fluidized grains. (3) The velocity of fluidized grains is always equal to the fluid velocity. (4) The fluid is incomprehensible and the solid grain is rigid.

Basic definitions: (1) The volume fraction of the α phase is $n^a = \mathrm{d}V^a/\mathrm{d}V$, where the α phase represents the solid grain phase, fluid phase, or fluidized grain phase; $\mathrm{d}V^a$ is the volume of the α phase; and $\mathrm{d}V$ is the volume element of three-phase medium. (2) The partial density of the three phases is defined as $\rho^a = \mathrm{d}m^a/\mathrm{d}V$, where $\mathrm{d}m^a$ is the mass of α phase. (3) The real density of the α phase is $\rho^{\alpha'} = \mathrm{d}m^a/\mathrm{d}V^a$, for which the fluidized grain phase shares the same real density with solid grain phase; $\rho^{sg'} = \rho^{fs'} = \rho^{s'}$, $\rho^{s'}$ is the real density of soil particles, and $\rho^{f'}$ is the real density of the fluid. (4) The porosity φ and the concentration c of the fluidized grains in the fluid are defined as $\varphi = \mathrm{d}V_V/\mathrm{d}V = n^f + n^{fs}$ and $c = \mathrm{d}V_{fs}/\mathrm{d}V_V = n^{fs}/(n^f + n^{fs})$, respectively, where $\mathrm{d}V_V$ is the pore volume.

Mass balance equation

For a multiphase flow system, the mass balance equation can be expressed as follows (Bear 1972):

$$\frac{\partial \rho^a}{\partial t} + \mathrm{div}(\rho^a \mathbf{v}^{a'}) = \dot{m}^a \tag{1}$$

where $\mathbf{v}^{a'}$ is the real velocity of the α phase, the term $\dot{m}^a$ on the right-hand side of equation (1) represents the mass generation rate of the α phase, the first term on the left is the partial density change rate of the α phase, and the second term represents the net accumulation term of the α phase.

According to the Dupuit–Forchheimer law (Bear 1972), the volume discharge $\mathbf{q}$ of the fluid–particle mixture is related to the velocity $\mathbf{v}$ as follows:

$$\mathbf{v} = \mathbf{q}/\varphi \tag{2}$$

Therefore, the mass balance equations of the three phases are as follows:

Solid grains phase:

$$\frac{\partial \varphi}{\partial t} = \frac{\dot{m}}{\rho_s} \tag{3}$$

Fluidized grains phase:

$$\frac{\partial(c\varphi)}{\partial t} + \nabla \cdot (c\mathbf{q}) = \frac{\dot{m}}{\rho_s} \tag{4}$$

Fluid phase:

$$\nabla \cdot \mathbf{q} = 0 \tag{5}$$

where $\dot{m}$ represents the rate of produced mass (here removed due to erosion).

Equations (3)–(5) constitute a set of three mass balance equations for the three considered phases of completely weathered granite. There are four independent unknown variables φ, c, $\mathbf{q}$, and $\dot{m}$; thus, one additional equation is necessary for solving this erosion problem. Therefore, a porosity evolution law is established in the following section.

Porosity evolution law

The evolution mechanism of mass transfer includes washout effect, abrasive effect, and corrosion (Feng, Chen, and Li 2001, Feng, Li, and Chen 2004; Wang 2014). The main minerals of completely weathered granite include quartz particles and clay minerals such as kaolinite and montmorillonite. Under the chemical reaction of water, these minerals will dissolve at different levels, and cause rock corrosion to generate the fine particles. Meanwhile, under the action of water washout, the fine particles will migrate and drive the coarse particles to generate new fine particles due to the abrasive effect. With the progress of corrosion, washout, and abrasive effect, the particle loss or mass transfer will continuously occur and lead to the change of porosity at last.

For mass transfer or erosion problem in porous media, many scholars have performed extensive theoretical and experimental studies since 1990s (Vardoulakis, Stavropoulou, and Papanastasiou 1996; Stavropoulou et al. 1998). These works, summarized in the paper by Rahmati et al. (2013), resulted in many constitutive equations that govern the erosion process. These ideas are adopted to describe the process of piping and sand production in the form of a porosity evolution law for the rate of eroded mass as follows:

$$\frac{\partial \varphi}{\partial t} = \dot{m}/\rho_s = (\dot{m}_{er} - \dot{m}_{dep})/\rho_s = \lambda(1 - \varphi)(c - c^2/c_{cr})|q| \tag{6}$$

where λ is the coefficient of the porosity evolution equation, $|q|$ is the module of volume discharge q, $\dot{m}_{er}$ is the rate of eroded mass, $\dot{m}_{er} = \rho_s\lambda(1 - \varphi)c|q|$, where $\dot{m}_{dep}$ is the rate of deposited mass, and $\dot{m}_{dep} = \rho_s\lambda(1 - \varphi)|q|c^2/c_{cr}$, where c_{cr} is a critical value of c for which the two competing phenomena, erosion and deposition, balance each other.

However, water inrush has some differences with piping and sand production because both the fine and coarse particles will be eroded. This leads to the concentration c of fluidized grains being higher than piping and sand production. Moreover, the fast fluid velocity will result in a much higher rate of eroded particle mass, greater than the rate of deposited mass for water inrush. Therefore, Eq. (6) will be simplified as follows by ignoring the deposition phenomena.

$$\frac{\partial \varphi}{\partial t} = \lambda(1 - \varphi)c|q| \tag{7}$$

From Eq. (7), the derivation of porosity is proportional to the concentration c. If c is nonzero, the erosion process, modeled by such a law, will run until all of the mass is eroded away, namely, the porosity $\varphi = 1$. However, Hu and Ma (2013) and Zhang et al. (2014b) conducted seepage erosion experiments and showed that the collapse or water inrush occurred before the porosity $\varphi = 1$. A maximum stability porosity was observed in the erosion process, at which point, the seepage–erosion process became stable, mass transfer did not occur and the porosity remained unchanged. Thus, for Eq. (7), considering the maximum porosity, the porosity evolution equation (7) needs to be further modified as follows:

$$\frac{\partial \varphi}{\partial t} = \lambda(\varphi_m - \varphi)c|q| \tag{8}$$

where φ_m is the maximum porosity of completely weathered granite, which is related to the physical properties of the medium, particle size distribution, and stress state. Through the study of seepage–erosion coupled experiments and internal soil erosion (Bendahmane, Marot, and Alexis 2008; Chang and Zhang 2011), the relationship between maximum porosity and physical and mechanical properties was concluded as follows:

$$1/(\varphi_m - \varphi_0) = a + b/|i| \tag{9}$$

where φ_0 is the initial porosity, $|i|$ is the module of the hydraulic gradient i, and the parameters a and b need to be determined experimentally, which reflects the influences of medium physical properties and stress state. The final adoptive porosity evolution equation for water inrush can be expressed as follows:

$$\frac{\partial \varphi}{\partial t} = \lambda[(\varphi_0 + 1/(a + b/|i|)) - \varphi]c|q| \tag{10}$$

Water inrush mechanism and coupled seepage equations

Water inrush in completely weathered granite is a coupled seepage–erosion process. The evolution process of water inrush can be divided into three stages: (1) the initial linear flow stage in which the fluid flow is very slow at the beginning, and flow is a linear laminar flow; (2) the rapid flow stage in which the porosity is obviously increased with the loss of particles, thus leading to a rapidly increasing flowing velocity; and (3) the pipe flow stage, which occurs after the formation of the water inrush channel in which the flow transforms into pipe flow.

Darcy's law, ignoring the inertial force, is suitable for porous medium of low permeability in the initial linear flow stage of water inrush. Darcy's law takes the following form:

$$\mathbf{q} = -\frac{k}{\eta_k \bar{\rho}} \nabla(p + \bar{\rho}gZ) \tag{11}$$

where p is the pore pressure, η_k is the kinematic viscosity of the fluid, Z is the height, g is the acceleration of gravity, and $\bar{\rho}$ is the real density of fluid and fluidized grain mixture; $\bar{\rho} = c\rho^{s'} + (1 - c)\rho^{f'}$. k is the intrinsic permeability of the porous medium. In addition, the permeability k can be expressed by the porosity using Kozeny–Carman formula:

$$k = k_0 \left(\frac{\varphi}{\varphi_0}\right)^3 / \left(\frac{1 - \varphi}{1 - \varphi_0}\right)^2 \tag{12}$$

where k_0 is the initial permeability of porous media.

For the rapid flow stage, the Brinkman's equation considered the shear stress of viscous fluid in the fast-moving fluid, so that it can be more suitable for describing the flow of fast-moving fluid in high porosity medium. The equation is expressed as follows (Brinkman 1949):

$$\left. \begin{array}{l} (\eta_k/k)\mathbf{q} = \nabla \cdot [-p\mathbf{I} + \eta_k(\nabla\mathbf{q} + (\nabla\mathbf{q})^T)] + \mathbf{F} \\ \nabla\mathbf{q} = 0 \end{array} \right\} \tag{13}$$

where $\mathbf{F}$ is the body force term and $\mathbf{I}$ is the unit matrix.

After the formation of water inrush channel, the fluid flow is dominated by kinetic energy, and the fluid flow is similar to pipe flow. Obviously, the Navier–Stokes equation is suitable for this stage. The Navier–Stokes equation takes the following form:

$$\bar{\rho}(\mathbf{q}\cdot\nabla)\mathbf{q} = \nabla[-p\mathbf{I} + \eta_k(\nabla\mathbf{q} + (\nabla\mathbf{q})^T)] + \mathbf{F} \left.\right\} \tag{14}$$
$$\nabla\cdot\mathbf{q} = 0$$

To depict the change in flow pattern in the whole time evolution process of water inrush, a coupled Darcy–Brinkman–Navier–Stokes equation was established based on the above analysis. The coupled equation for porous media can be expressed as follows:

$$\frac{\bar{\rho}}{\varphi}\left(\mathbf{q}\cdot\nabla\frac{\mathbf{q}}{\varphi}\right) = \nabla\cdot(-p\mathbf{I})$$
$$+ \nabla\left\{\frac{1}{\varphi}[\eta_k(\nabla\mathbf{q} + (\nabla\mathbf{q})^T) - \frac{2\eta_k}{3}(\nabla\cdot\mathbf{q})\mathbf{I}]\right\}$$
$$- \frac{\eta_k}{k}\mathbf{q} + \mathbf{F}\nabla\cdot\mathbf{q} = 0 \tag{15}$$

The left term in Eq. (15) is the inertia term of the Navier–Stokes equation. The second term on the right denotes the viscous term of Brinkman's model, and the third term is the viscous term of Darcy's law.

It can be observed from Eq. (15) that the equation can simplify to Darcy's equation by neglecting the inertia term and the viscous term of Brinkman's equation when the flow velocity is very small. As the evolution process enters into rapid flow stage, it has the advantage of approximating equation (13) when the viscous term of Brinkman's law plays a major role. When the channel has formed, the inertia term of Navier–Stokes will obviously increase, and the equation can approximate to Eq. (14) to describe the third stage.

The basic unknowns in the coupled seepage erosion water inrush equations (3)–(5), (10), (12), and (15) are only p, c, and φ. Combining the relative initial conditions and boundary conditions, these partial differential equations (PDE) can be solved numerically by adopting the Galerkin finite method and implicit difference method to discretize space and time. Considering the nonlinearity of the equation system, the solution can be obtained with the Newtown–Raphson iteration method. With these methods, the COMSOL multiphysics system was adopted to solve these PDE equations by secondary development in this paper.

Numerical simulation

Example 1

In petroleum engineering, sand production can lead to various problems, such as wellbore instability and the formation of unstable cavities in the geological formation. Stavropoulou et al. (1998) presented a sand production prediction model in 1998. Based on this model, Luo (2013) presented a backward erosion piping model. The piping channel will appear when the fine particles are continually dislodged from the soil matrix. In fact, water inrush in completely weathered granite is
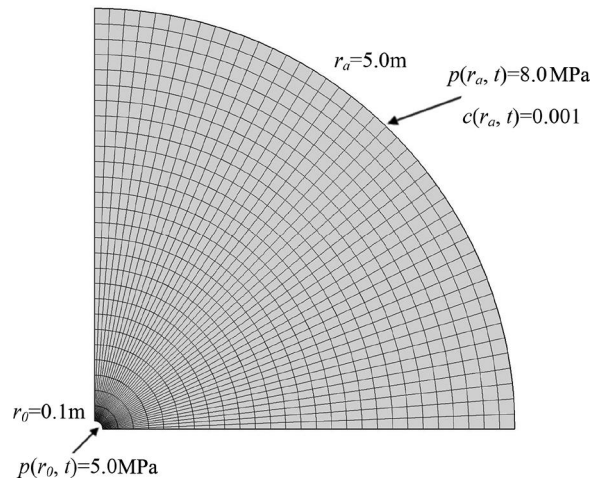

Figure 1. Finite element model for the Example 1.

similar to the sand production and piping, especially the piping. In the evolution process of water inrush, particles, including both fine and coarse particles, are progressively eroded through tractive force caused by seepage water, thus leading to the formation of unstable cavities until the water inrush channel is transfixed.

To verify the effectiveness of the developed water inrush model, comparisons with the results from the newly developed model with those from the sand production and backward erosion piping model were presented to describe the wellbore erosion phenomena. Figure 1 shows the finite element model, with a wellbore radius of $r_0 = 0.1$ m and an outer boundary radius of $r_a = 5$ m. The boundary conditions and physical parameters of this model are stated in Table 1. The computing time is 8,000 s. Figure 2 shows the variation of porosity and fluidized grain concentrations at the free surface ($r = r_0$) with time, Figure 3 demonstrates the spatial profiles of porosity and pore pressure at $t = 6,800$ s, and Figure 4 depicts the field variable distributions at $t = 3,000$ and 8,000 s.

It is observed from Figure 2 that the results from the developed model are consistent with the results of Stavropoulou et al. (1998) and Luo (2013). The porosity and fluidized grain concentration at the free surface increase slowly until 2,000 s, and then both increase rapidly from 0.28 and 0.02 to 0.91 and 0.25, respectively, between 2,000 and 7,000 s and increase gradually again after 7,000 s. The porosity tends to the maximum value of 1.0, and the fluidized grain concentration finally converges to the critical value of 0.3.

Figure 3 shows that the results from the developed model are consistent with those of Stavropoulou et al. (1998) and Luo

Table 1. Physical parameters of Example 1.

|	
Initial porosity $\varphi(r, 0)$	0.25
Initial fluidized grain concentration $c(r, 0)$	0.001
Fluidized grain concentration on the outer boundary $c(r_a, t)$	0.001
Wellbore fluid pressure $p(r_0, t)$	5 MPa
Pore pressure on the outer boundary $p(r_a, t)$	8 MPa
Coefficient λ	5 m^{-1}
Parameter a	1.533
Parameter b	153.4
Real density of fluid $\rho^{f'}$	840 kg m^{-3}
Real density of grains $\rho^{s'}$	2,650 kg m^{-3}
Kinematic viscosity of the fluid η_k	5×10^{-6} m^2 s^{-1}
Initial permeability k_0	1.3×10^{-11} m^2
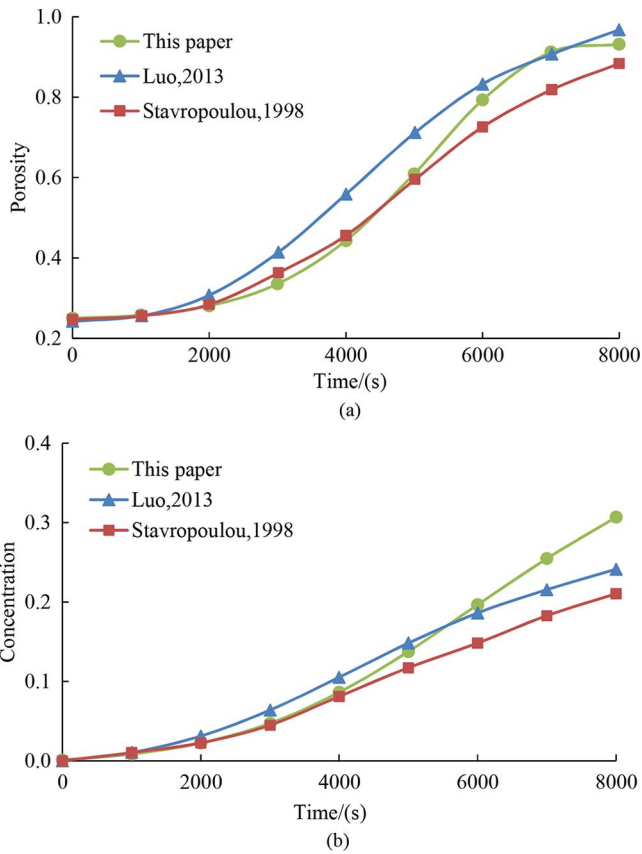
Figure 2. Time variation of porosity and fluidized grain concentration at free surface. (a) Porosity and (b) fluidized grain concentration.
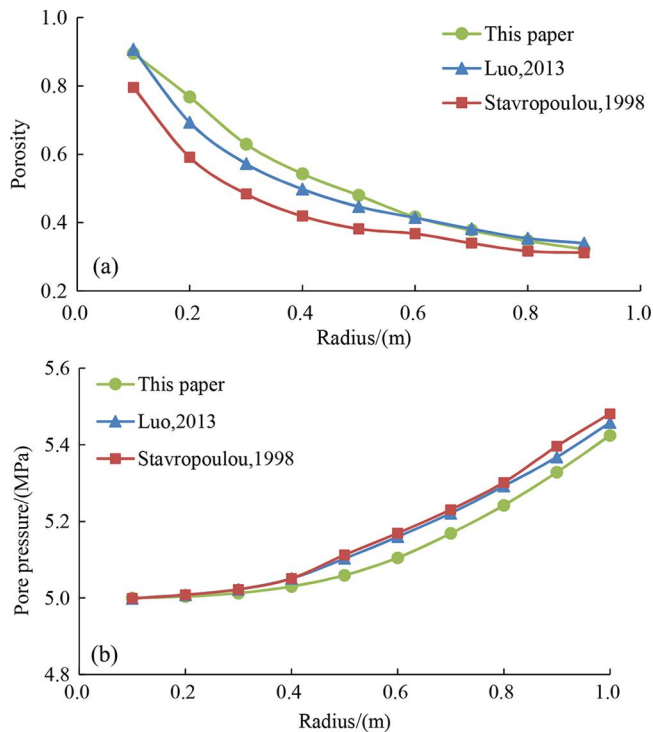

Figure 3. Spatial profiles of porosity and pore pressure at $t = 6{,}800$ s. (a) Porosity and (b) pore pressure.

(2013). The porosity near the free surface is more easily changed, and it is rapidly diminished within a small distance. This indicates that the erosion near the free surface is more serious, which in turn results in a lower pressure gradient in the eroded region.

Figure 4 shows that the porosity and fluidized grain concentration increase rapidly close to the free surface; however, far away from the free surface, both diminish rapidly to the initial values. The variation of pore pressure is obviously different from that of porosity and fluidized grain concentration; the pore pressure gradient close to the free surface sharply changes in the beginning, and then it gradually transitions to a linear distribution.

Example 2

To study the nonlinear water inrush mechanism and compare the effects of Darcy and coupled seepage equations proposed above on the water inrush mechanism, the evolution of water inrush in the tunnel floor and completely weathered granite geological formation is presented in Example 2 as shown in Figure 5, which is referred to as floor water inrush. This is a common type of water inrush disaster in tunnels and underground engineering.

Table 2 shows the physical parameters. The initial conditions were as follows: porosity $\varphi(r, 0) = 0.1$, fluidized grain concentration $c(r, 0) = 0.01$. The initial pore pressure of the entire region was obtained from the initial steady seepage calculation. The boundary conditions were as follows: the pore pressure at the outlet and inlet boundaries was 0 and 2 MPa, respectively. The computing time is 1,000 s. Figures 6–11 show the time variation of various variables at monitoring point B.

Figure 6 shows that the Reynolds number changes from less than 100 to over 48,000 for the coupled seepage model. This indicates that the flow pattern has multiple transformations during the evolution of seepage erosion process. Kong (1999) showed that the critical Reynolds number between turbulent flow and laminar flow is 100 for porous medium. The flow is laminar or at the laminar–turbulent transition, which is mainly governed by laminar flow, when the Reynolds number is lower than 100. However, with regard to the pipe flow when the water channel is formed, Erhard et al. (2010) declared that the critical Reynolds number between turbulent flow and laminar flow was 2,000–4,000, and the Reynolds number of steady turbulent flow is 4,000. Therefore, according to the critical Reynolds number in porous medium flow and pipe flow, the evolution of water inrush of Example 2 was divided into three stages, as shown in Figure 6. That is, the Darcy stage with a Reynolds number of less than 100 (A_1 to A_2), the Brinkman stage with a Reynolds number between 100 and 4,000 (A_2 to A_3), and the Navier–Stokes stage with a Reynolds number over 4,000 (A_3 to A_4).

Figures 7 and 8 show that the evolution of pore pressure and flow velocity continuously changes with time. The largest variation of the velocity gradient mainly occurs in the Brinkman stage, and the largest variation of the pressure gradient mainly occurs in the Darcy stage and Brinkman stage, whereas the variation of pressure gradient changes little when the evolution process enters into the Navier-Stokes stage. This indicates that the seepage resistance in the Darcy and
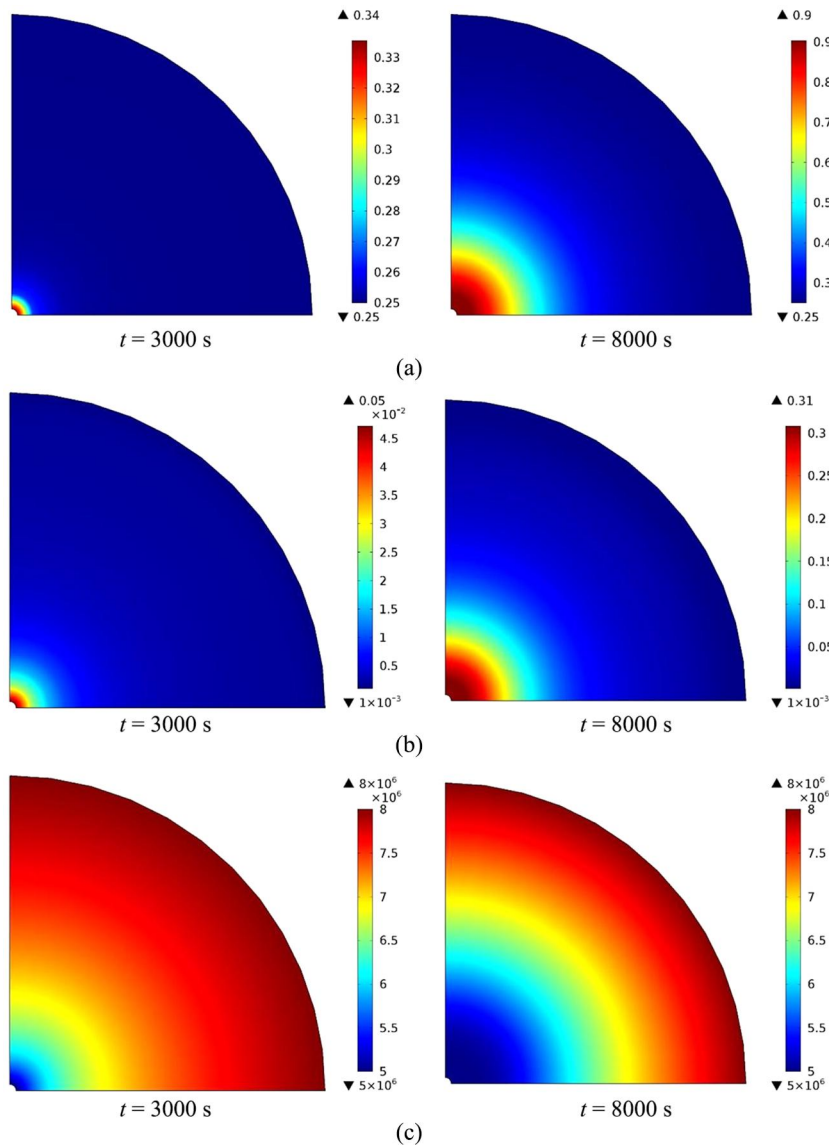
Figure 4. Contours of field variables at $t = 3,000$ s and $t = 8,000$ s. (a) Porosity, (b) fluidized grain concentration, and (c) pore pressure (unit: Pa).

Brinkman's stages is higher in the evolution process. In the Darcy stage, the flow velocity is very small, i.e., the maximum velocity is only 0.0019 m s^{-1}, and the maximum velocity increases 118 times to 0.227 m s^{-1} as the process enters into the Brinkman stage. In the Navier–Stokes stage, the velocity increases continually to 0.368 m s^{-1}. This rapid and periodic change in the flow velocity can better reflect the nonlinear change in water flow in the evolution of water inrush.

Compared to the coupled seepage model, the velocity and pore pressure have an obvious jump in the rapid evolution stage of porosity when the calculation uses the Darcy seepage model. It cannot effectively describe the smooth transition of the evolution process. Furthermore, the final flow velocities of the Darcy seepage model and coupled seepage model are 1.47 and 0.39 m s^{-1}, respectively. This is because the Darcy

seepage model only considers the seepage resistance and ignores the shear resistance in the rapid flow stage and the inertia term in the pipe flow stage. Thus, the water inrush
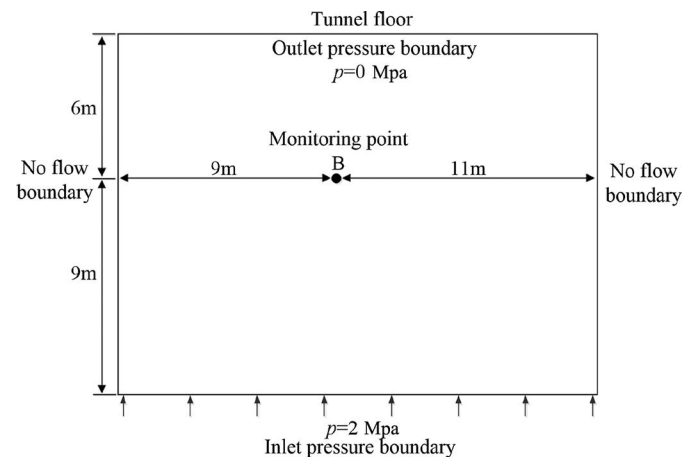

Figure 5. Floor water inrush model for the Example 2

Table 2. Physical parameters of Example 2.

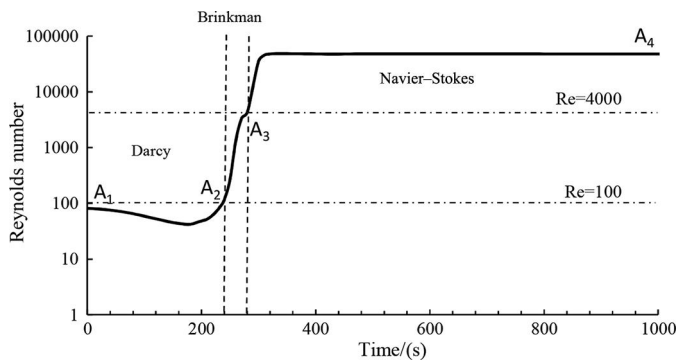| k_0/m^2	η_k (m^2 s^{-1})	$\rho^{f'}$ (kg m^{-3})	$\rho^{s'}$ (kg m^{-3})	λ (m^{-1})	a	b
5×10^{-12}	1×10^{-6}	1,000	2,650	5	1.533	153.4

Figure 6. Time variation of Reynolds number at point B for coupled seepage model.

Figure 7. Time variation of pore pressure at point B.

Figure 9. Time variation of porosity at point B.
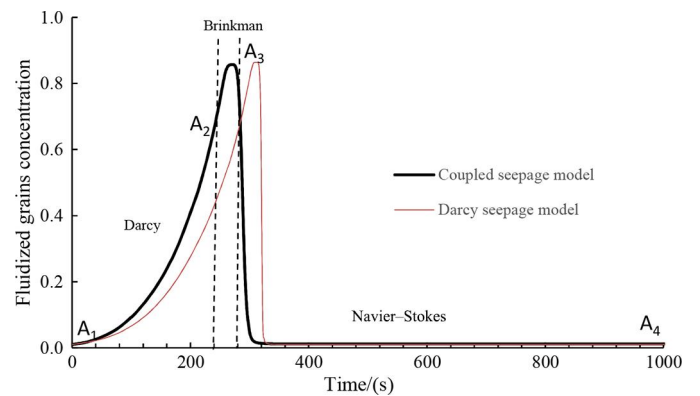
Figure 10. Time variation of fluidized grains concentration at point B.
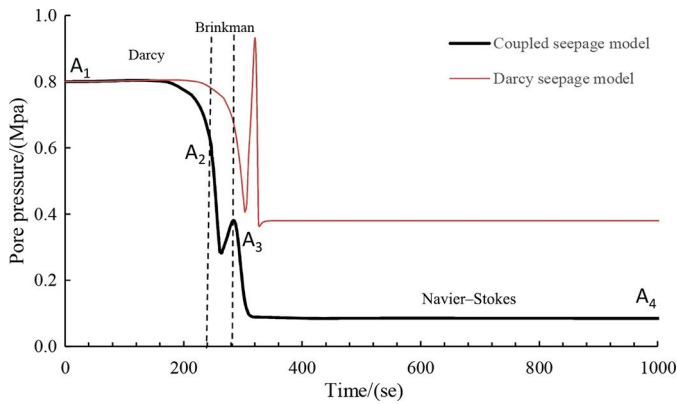
model only using Darcy's law was obviously larger than the real conditions.

Figure 9 indicates that the change in porosity in the Brinkman stage is the largest. This is because the change in the hydraulic gradient and seepage velocity in this stage is the most significant, and the erosion in this stage is also the most serious.

Figure 10 shows that the change in fluidized grain concentration is more complicated than that of porosity. The fluidized grain concentration continuously increases before the Brinkman stage, and the maximum concentration is achieved in the Brinkman stage, at which point, the concentration starts
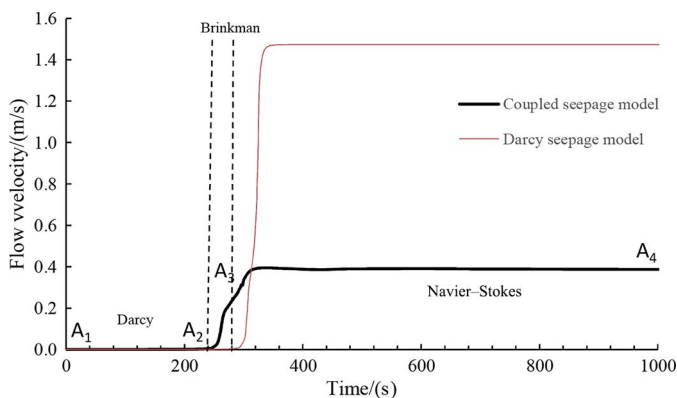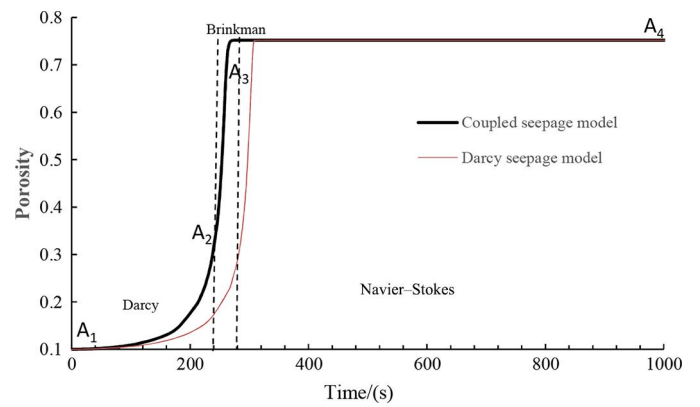
to decrease in the Navier–Stokes stage. The fluidized grain concentration c consists of convection and mass generation. An increase in the fluidized grain concentration with time indicates that the erosion process becomes more active than the transport process until the point where the convection overtakes the mass generation. On the contrary, it indicates
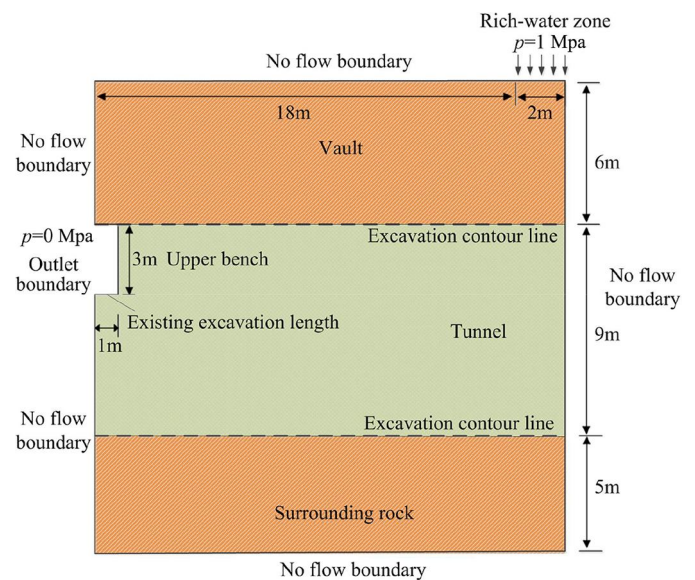

Figure 8. Time variation of flow velocity at point B.

Figure 11. Tunnel water inrush model for the Example 3.

Table 3. Physical parameters of Example 3.

k_0/m^2	η_k (m^2 s^{-1})	$\rho^{f'}$ (kg m^{-3})	$\rho^{s'}$ (kg m^{-3})	λ (m^{-1})	a	b
5×10^{-12}	1×10^{-6}	1,000	2,650	5	1.533	153.4

that the erosion process has almost been completed and that the water inrush channel has formed when the concentration tends to decrease. This is also a mutual verification between the change in fluidized grain concentration and flow pattern.

Compared with the Darcy seepage model and the coupled seepage model, it can be observed from Figures 9 and 10 that there is not an obvious influence on the values of porosity and fluidized grain concentration. The influences on the porosity and fluidized grain concentration are mainly from the evolution rate and mutation time. The evolution rates of the porosity and fluidized grain concentration in the coupled seepage model are larger than those of the Darcy seepage model, and the mutation time of the coupled seepage model is also much shorter.

In summary, the numerical results show that pore pressure, flow velocity, evolution rates of porosity, fluidized grain

concentration, and mutation time of the Darcy seepage model and coupled seepage model are quite different, and the newly developed model is more practical.

Example 3

The three-bench method is a common tunnel excavation method in geology, particularly for water-rich completely weathered granite strata. During the excavation of the upper bench, it is easy to cause water inrush disasters, especially when there is abundant groundwater with high pressure in the tunnel vault (Li et al. 2014). Therefore, the evolution of water inrush in completely weathered granite strata with high water content and water pressure is presented in Example 3.

Figure 11 shows the geometry and finite element model. The height of the upper bench is 3 m, and the existing excavation length is 1 m. There is a water-rich zone with high water pressure in the tunnel vault, with a length and height of 18 and 6 m, respectively, from the tunnel face. Table 3 shows the physical parameters. The initial conditions are
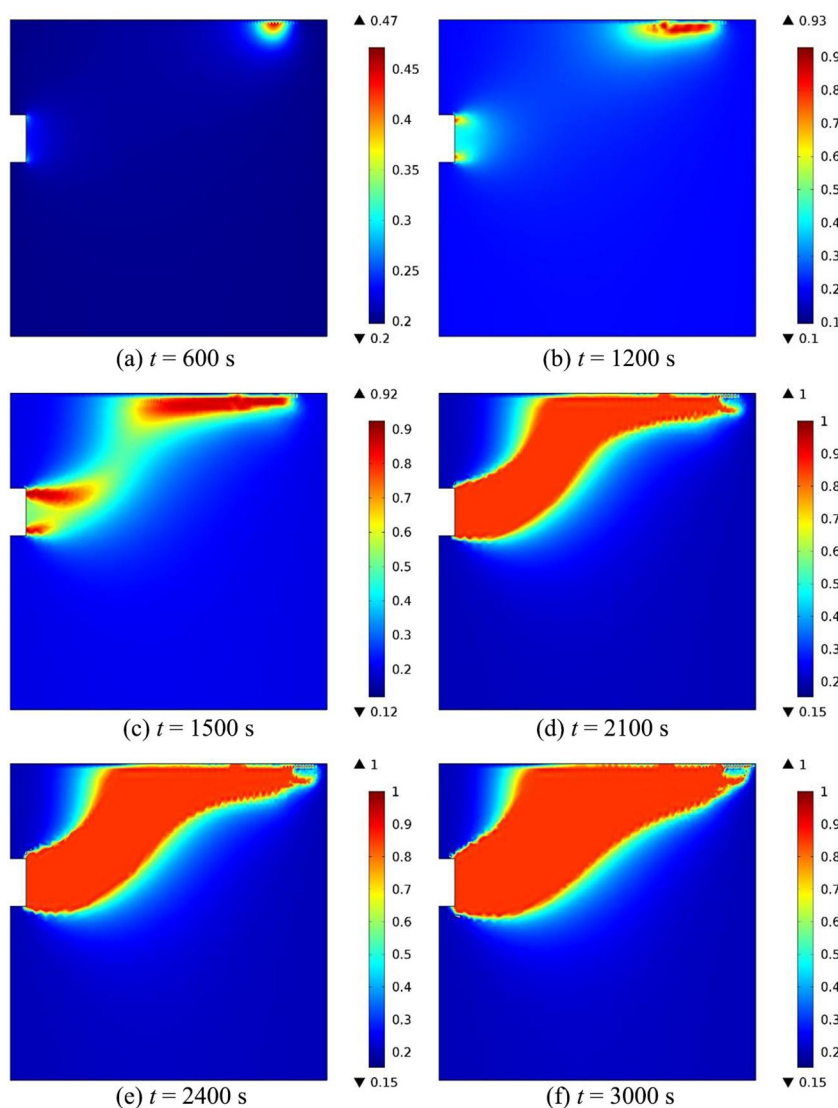

Figure 12. Time variation of porosity. (a) $t = 600$ s, (b) $t = 1,200$ s, (c) $t = 1,500$ s, (d) $t = 2,100$ s, (e) $t = 2,400$ s, and (f) $t = 3,000$ s.
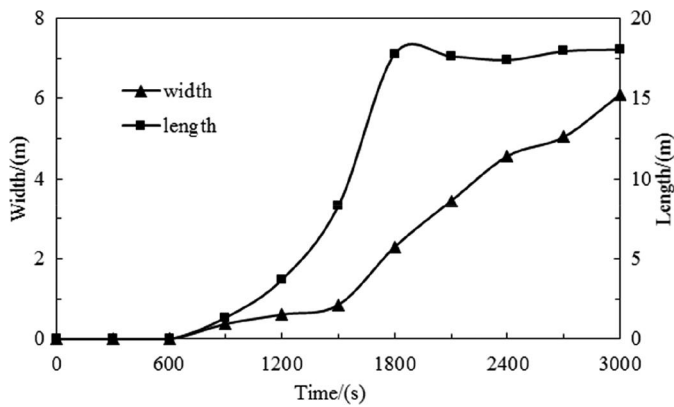
Figure 13. Time variation of average channel size.

Figure 14. Spatial profile of flow velocity at $t = 3,000$ s (unit: m s^{-1}).

as follows: porosity $\varphi(r, 0) = 0.2$, fluidized grain concentration $c(r, 0) = 0.01$; the initial pore pressure of the entire region was obtained from the initial steady seepage calculation. The boundary conditions are as follows: the water pressures of the water-rich region in the tunnel vault and outlet boundary of tunnel face are 1 and 0 MPa, respectively. The computing time is 3,000 s. Figures 12, 13 show the time variation of porosity, fluidized grain concentration, and size of the water inrush channel, respectively. Figure 14 depicts the spatial contours of the water flow velocity at $t = 3,000$ s.

Figure 12 shows that the change in porosity is high near the exit and in the water-rich zone and that it diminishes rapidly within a small distance when the evolution time is less than 1,200 s, and the maximum porosity at the exit and water-rich zone is close to 1. This indicates that the erosion process is more active close to the exit and water-rich zone, and considerable particle loss and even the formation of unstable cavities in this area have occurred. As the evolution continues, the development of porosity increases between the exit and water-rich zones (Figure 12c), and the region that the porosity is larger than 0.8 will transfix quickly, as shown in Figure 12d. This indicates that the water inrush channel has formed. Furthermore, the formation of water inrush channel aggravates the development of erosion due to the increase in flow velocity. The channel width increases with the continual erosion, as shown in Figure 12e and 12f.

Figure 13 shows the time evolution of average channel size. The channel or cavity was defined as having porosity over 0.8. In the beginning, the width and length of the channel are very small due to the weak erosion. From 0 to 1,800 s, the main development is the length of channel, which increases rapidly from zero until the transfixion of the channel. After the formation of channel, the length remains stable and the width increases rapidly from 0.8 to 6 m.

Figure 14 shows the spatial profile of the flow velocity at $t = 3,000$ s. It is observed from Figure 14 that the velocity in the channel is much larger than the other region; the maximum velocity is over 1.6 m s^{-1}. This indicates that the large amount of tunnel water is mainly flow in the channel. Undoubtedly, water inrush disaster probably has occurred with this sort of large channel.

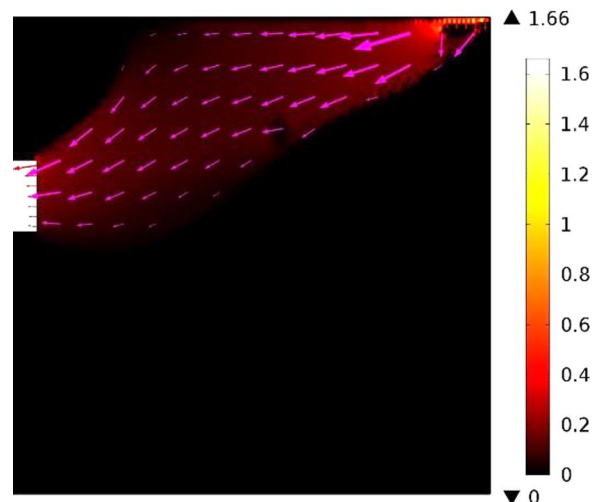The particle loss caused by seepage erosion is very significant in the evolution of water inrush, which has been

embodied in the seepage erosion water inrush model, so it is concluded that this proposed model has great advantages in predicting the development of water inrush channels.

Conclusion

Based on theories of solute transport and dynamics of fluids in porous media, a nonlinear coupled seepage erosion water inrush model was proposed in a completely weathered granite stratum, which consists of mass balance equations, coupled seepage equation, and porosity evolution law for the fluid flux of eroded particles. This model considers the features of particle loss and the change of flow patterns in the evolution of water inrush. It can predict the water inrush development under complex boundary and flow conditions; reflect the dynamic evolution of particle loss, porosity, permeability, pore pressure, and water inflow induced by the mass transfer of particles; and describe the unsteady, progressive failure features of water inrush. These improvements make up for the shortage of existing research on water inrush mechanism modeling and provide a new method for the design of prevention measures of water inrush such as curtain grouting technology.

However, some deficiencies of this new model still need to be improved in the future: (1) the new model cannot be used to predict the water inrush of fractured rock masses or in transition zones of rock and soil; establishment of a suitable water inrush model for these areas should be addressed in future studies. (2) The model in this paper does not adequately consider the mechanical effects. In fact, the erosion and particle loss will change the pore distribution and eventually cause changes in the stress state and shear strength, which may induce significant deformation or even collapse. The author is currently conducting an experimental study of nonlinear water inrush mechanisms based on a self-designed water inrush test apparatus that can control the confining pressure and water pressure. It is hoped that a modified nonlinear seepage–erosion–stress coupling water inrush mechanism will be proposed in the future.

Funding

ORCID

Jinquan Liu 　 http://orcid.org/0000-0003-2326-0684

References

Anon. 1977. The description of rock masses for engineering purpose: Working party report. *Quarterly Journal of Engineering Geology & Hydrogeology* 10:355–88. doi:10.1007/bf00584456

Arıkan, F., R. Ulusay, and N. Aydın. 2007. Characterization of weathered acidic volcanic rocks and a weathering classification based on a rating system. *Bulletin of Engineering Geology and the Environment* 66 (4):415–30. doi:10.1007/s10064-007-0087-0

Bear, J. 1972. *Dynamics of fluids in porous media*. New York: American Elsevier.

Bendahmane, F., D. Marot, and A. Alexis. 2008. Experimental parametric study of suffusion and backward erosion. *Journal of Geotechnical and Geoenvironmental Engineering* 134:57–67. doi:10.1061/(asce)1090-0241(2008)134:1(57)

Brinkman, H. C. 1949. A calculation of the viscous force exerted by a flowing fluid on a dense swarm of particles. *Applied Scientific Research* 1:27–34. doi:10.1007/bf02120313

Chang, D. S. and L. M. Zhang. 2011. A stress-controlled erosion apparatus for studying internal erosion in soils. *Geotechnical Test Journal* 34:579–89. doi:10.1520/gtj103889

Erhard, P., D. Etling, U. Muller, U. Riedel, K. R. Sreenivasan, and J. Warnatz. 2010. *Prandtl-essentials of fluid mechanics*. New York: Springer Science & Business Media.

Feng, X. T., S. Chen, and S. Li. 2001. Effects of water chemistry on microcracking and compressive strength of granite. *International Journal of Rock Mechanics & Mining Sciences* 38 (4):557–68. doi:10.1016/s1365-1609(01)00016-8

Feng, X. T., S. J. Li, and S. L. Chen. 2004. Effect of water chemical corrosion on strength and cracking characteristics of rocks - A review. *Key Engineering Materials* 261–263:1355–60. doi:10.4028/www.scientific.net/kem.261-263.1355

Hu, Y. Y. and P. Ma. 2013. Mechanism study and finite element simulation of three-phase coupling seepage erosion piping. *Rock and Soil Mechanics* 34:913–21. doi:10.3724/sp.j.1008.2012.00974

Irfan, T. Y. 1997. Mineralogical and fabric characterization and classification of weathered volcanic rocks in Hong Kong special project report SPR 1/97. Geotechnical Engineering Office, Hong Kong Government. Report number: SPR1/97. http://www.cedd.gov.hk/eng/publications/geo_reports/doc/er66.pdf

Kong, X. Y. 1999. *Advanced mechanics of fluids in porous media*. Hefei, China: University of Science and Technology of China Press.

Li, S. C., W. J. Zhang, Q. S. Zhang, X. Zhang, R. T. Liu, G. M. Pan, and Z. Y. Che. 2014. Research on advantage-fracture grouting mechanism and controlled grouting method in water-rich fault zone. *Rock and Soil Mechanics* 35 (3):744–52.

Li, S. C., Z. Q. Zhou, L. P. Li, Z. H. Xu, Q. Q. Zhang, and S. S. Shi. 2013. Risk assessment of water inrush in karst tunnels based on attribute synthetic evaluation system. *Tunnelling & Underground Space Technology* 38:50–58. doi:10.1016/j.tust.2013.05.001

Luo, Y. L. 2013. A continuum fluid-particle coupled piping model based on solute transport. *International Journal of Civil Engineering* 11 (1B):38–44.

Meng, Z., G. Li, and X. Xie 2012. A geological assessment method of floor water inrush risk and its application. *Engineering Geology* 143:51–60. doi:10.1016/j.enggeo.2012.06.004

Rahmati, H., M. Jafarpour, S. Azadbakht, A. Nouri, H. Vaziri, D. Chan, and Y. Xiao. 2013. Review of sand production prediction models. *Journal of Petroleum Engineering* 2013:1–16. doi:10.1155/2013/864981

Shin, J. H., K. C. Choi, J. U. Yoon, and Y. J. Shin. 2011. Hydraulic significance of fractured zones in subsea tunnels. *Marine Georesources & Geotechnology* 29 (3):230–47. doi:10.1080/1064119x.2011.555712

Shirlaw, J. N. 2016. Pressurised TBM tunnelling in mixed face conditions resulting from tropical weathering of igneous rock. *Tunnelling & Underground Space Technology* 57:225–40. doi:10.1016/j.tust.2016.01.018

Shirlaw, J. N., S. R. Hencher, and J. Zhao. 2000. Design and construction issues for excavation and tunnelling in some tropically weathered rocks and soils. ISRM International Symposium. Melbourne, Australia: International Society for Rock Mechanics.

Stavropoulou, M., P. Papanastasiou, and I. Vardoulakis. 1998. Coupled wellbore erosion and stability analysis. *International Journal for Numerical and Analytical Methods in Geomechanics* 22:749–69. doi:10.1002/(sici)1096-9853(199809)22:9<749::aid-nag944>3.3.co;2-b

Tang, J., H. Bai, B. Yao, and Y. Wu. 2011. Theoretical analysis on water-inrush mechanism of concealed collapse pillars in floor. *International Journal of Mining Science and Technology* 21 (1):57–60. doi:10.1016/j.mstc.2010.12.005

Valko, P. and M. Economides. 1994. Propagation of hydraulically induced fractures—A continuum damage mechanics approach. *International Journal of Rock Mechanics & Mining Sciences* 31:221–29. doi:10.1016/0148-9062(94)90466-9

Vardoulakis, I., M. Stavropoulou, and P. Papanastasiou. 1996. Hydro-mechanical aspects of the sand production problem. *Transport in Porous Media* 22:225–44. doi:10.1007/bf01143517

Wang, L. Z. 2014. Accelerated experimental study on permeability for broken mudstone with mass loss. PhD thesis, China University of Mining and Technology, Xuzhou, China.

Wang, J. A. and H. D. Park. 2003. Coal mining above a confined aquifer. *International Journal of Rock Mechanics & Mining Sciences* 40:537–51. doi:10.1016/s1365-1609(03)00029-7

Wei, J. C., Z. J. Li, L. Q. Shi, Y. Z. Guan, and H. Y. Yin. 2010. Comprehensive evaluation of water-inrush risk from coal floors. *International Journal of Mining Science and Technology* 20 (1):121–25. doi:10.1016/s1674-5264(09)60172-1

Yang, Y. and F. Huang. 2007. Water source determination of mine inflow based on non-linear method. *Journal of China University of Mining &Technology* 36 (3):283–86.

Yang, T. H., J. Liu, W. C. Zhu, D. Elsworth, L. G. Tham, & C. A. Tang. 2007. A coupled flow-stress-damage model for groundwater outbursts from an underlying aquifer into mining excavations. *International Journal of Rock Mechanics & Mining Sciences* 44:87–97. doi:10.1016/j.ijrmms.2006.04.012

Zhang, D. L., Q. Fang, and H. C. Lou. 2014a. Grouting techniques for the unfavorable geological conditions of Xiang'an subsea tunnel in china. *Journal of Rock Mechanics and Geotechnical Engineering* 6 (5):438–46. doi:10.1016/j.jrmge.2014.07.005

Zhang, R., Z. Q. Jiang, H. Y. Zhou, C. W. Yang, and S. J. Xiao. 2014b. Groundwater outbursts from faults above a confined aquifer in the coal mining. *Natural Hazards* 71:1861–72. doi:10.1007/s11069-013-0981-7

Zhang, J. and B. Shen. 2004. Coal mining under aquifers in China: A case study. *International Journal of Rock Mechanics and Mining Sciences* 41 (4):629–39. doi:10.1016/j.ijrmms.2003.01.005

Zhao, J., Q. M. Gong, and Z. Eisensten. 2007. Tunnelling through a frequently changing and mixed ground: A case history in Singapore. *Tunnelling & Underground Space Technology* 22 (4):388–400. doi:10.1016/j.tust.2006.10.002

Zhao, Y., P. Li, and S. Tian. 2013. Prevention and treatment technologies of railway tunnel water inrush and mud gushing in China. *Journal of Rock Mechanics and Geotechnical Engineering* 5 (6):468–77. doi:10.1016/j.jrmge.2013.07.009